pp. 1–24 (2022)

Computational analysis of the impact of aortic bifurcation geometry to AAA haemodynamics

D. V. Tikhvinskii[*], L. R. Merzhoeva[*], A. P. Chupakhin[*], A. A. Karpenko[*,†], and D. V. Parshin[*]

Abstract — Abdominal aortic aneurysm is a widespread disease of cardiovascular system. Predicting a moment of its rupture is an important task for modern vascular surgery. At the same time, little attention is paid to the comorbidities, which are often the causes of severe postoperative complications or even death. This work is devoted to a numerical study of the haemodynamics of the model geometry for possible localizations of abdominal aortic aneurysm: on the aortic trunk or on its bifurcation. Both rigid and FSI numerical simulations are considered and compared with the model aortic configuration without aneurysm. It is shown that in the case of localization of the aneurysm on the bifurcation, the pressure in aorta increases upstream. Moreover, only in the case of a special geometry, when the radii of the iliac arteries are equal ($r_1 = r_2$), and the angle between them is 60 degrees, there is a linear relationship between the pressure in the aorta above the aneurysm and the size of the aneurysm itself: the slope of the straight line is in the interval $a \in (0.003; 0.857)$, and the coefficient of determination is $R^2 \geqslant 0.75$. The area bounded by the curve of the 'pressure–velocity' diagram for the values of velocity and pressure upstream in the presence of an aneurysm decreases compared to a healthy case (a vessel without an aneurysm). The simulation results in the rigid and FSI formulations agree qualitatively with each other. The obtained results provide a better understanding of the relationship between the geometrical parameters of the aneurysm and the changing of haemodynamics in the aortic bifurcation and its effect on the cardiovascular system upstream of the aneurysm.

Keywords: Abdominal aortic aneurysms, blood flow, haemodynamics, computational fluid dynamics, upstream effect, aortic bifurcation morphology, AAA comorbidities

MSC 2010: [MSC 2010]35Q92, 65M08, 76Zxx

The aorta is the largest blood vessel in the body and has a complex geometry: the ascending segment that exits from the heart, then the arch, following by the descending segment, consisting of thoracic and abdominal compartments, a long trunk with small but vital branches, and a branching (bifurcation) of the aorta into the iliac arteries in the abdominal compartment (see Fig. 1a). Almost every segment of the aorta is studied and operated on by separate medical stuff. In biomechanics, all these sections of the aorta are studied, but most of the work is devoted to its thoracic and abdominal segments. The thoracic aorta with an aneurysm is a long tube with a bulge, the parameters of which can be varied and various hydrodynamic

[*]Novosibirsk State University, Novosibirsk 630090, Russia

[†]Meshalkin National Medical Research Center, Novosibirsk 630055, Russia
E-mails: d.tikhvinskii@g.nsu.ru, l.merzhoeva@g.nsu.ru, parshin@hydro.nsc.ru

This work was supported by a grant from Russian Science Foundation, project No. 21-15-00091.

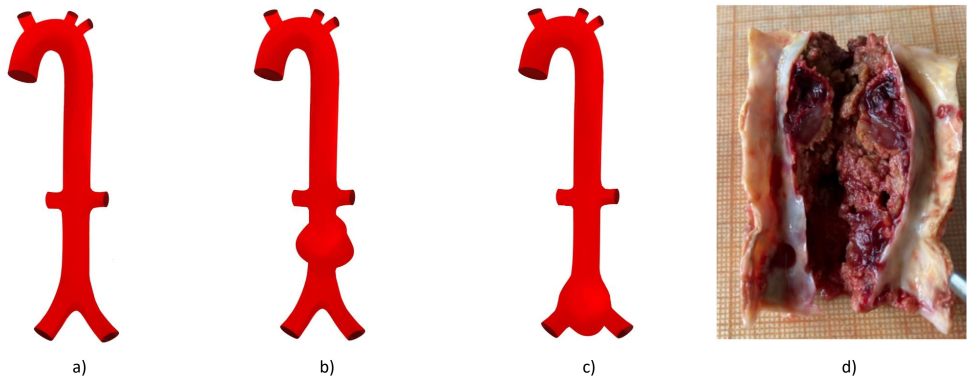

Figure 1. Schematic representation of (a) healthy aorta, (b) aorta with an abdominal aneurysm on the trunk, (c) aorta with an abdominal aneurysm on the bifurcation, (d) aneurysm of the abdominal aortic trunk after resection in section. Thrombotic masses are visible, which are almost completely blocking the lumen of the vessel. The blood flow was carried out through the exfoliated wall of the aorta.

quantities (pressure wave propagation velocity, phase shift in pulsating flows, etc.) can be considered (see, e.g., [3, 5]). In its abdominal segment, the aorta is directly adjacent to the spine, which is rigid and limits the pulsations of the aortic walls, which affects the blood flow in it. An aneurysm of the abdominal aorta (see Figs. 1b and 1c) can be located both directly on the aortic bifurcation when it branches to the iliac arteries, and at a distance of 5–10 cm above the bifurcation. This vascular pathology is quite common [60] and dangerous, since aneurysm rupture often leads to death even in a hospital setting. In addition, this pathology introduces significant deviations in the blood supply to the proximal (upstream) sections of the aorta and the organs that feed from its branches: the kidneys, intestines, and others. The blood flow in the aneurysm generates eddies that lead to the formation of blood clots in it. Separation of blood clots from the walls can lead to embolism (occlusion) of the vessels of the lower extremities. Partial embolism (partial occlusion of the vessel lumen by blood clots) is one of the markers in the diagnosis of abdominal aortic aneurysm (see Fig. 1d).

In the presence of an aneurysm on the affected walls of the aorta and iliac arteries, degenerative processes associated with remodelling of healthy tissue develop, its remodelling (increase in collagen content and loss of smooth muscle cells, restructuring of the ensemble of collagen and elastin fibers) [35]. A characteristic process is the formation of inclusions of calcifications of various scales [10], which entails an even greater change in both the strength properties of the vessel walls and the haemodynamics of the aorta. The task of studying an aneurysm of the abdominal aorta is complex, including both the hydrodynamic component and the problem of strength mechanics, as well as physiological aspects associated with the processes of thrombus formation and abnormalities of vascular tissues [45]. An important stage in the study of the complex system 'bifurcation-aneurysm' is mathematical and computer modelling, which allows to estimate the hydrodynamic quantities for various values of the system parameters. There is a large number of works devoted to this topic in various formulations [47, 51], as well as fundamental works on the principles of applying multiscale modelling for such pathologies [14]. Many studies are devoted to the use of personalized 3D modelling to find triggers for the risk of aneurysm rupture [15] and to develop a methodology for determining the location of the rupture [4]. However, due to the high variability of clinical data, when using personalized configurations, it can be difficult to separate the influence of specific geometric features of the vascular bed from the general effects arising due to more general geometric characteristics (aneurysm size, location relative to the bifurcation, iliac artery opening angle, etc.). We noted a similar trend while working with cerebral aneurysms [57], so we consider it useful to evaluate the effect of such parameters on the haemodynamics of aortic bifurcation with an aneurysm in idealized (model) configurations.

The work numerically simulates the influence and interaction of aortic bifurcation and its aneurysm on the hydrodynamics of blood flow in this system, and investigates the role that this interaction plays in the cardiovascular system of the upper aorta. The clinical value of the work is that its results can be used to develop new and modify existing criteria for assessing the risk of rupture. The point is that an aneurysm, even in a state that is not prone to rupture, can have an extremely negative effect on the haemodynamics of the aorta upstream to the heart, which can lead to severe and sometimes even critical complications during treatment.

1. Research methods

1.1. Construction of geometry

The first stage of work is digitalization, restoration of the 3D geometry of the abdominal aorta and iliac arteries. For this, computer tomography (CT) images in the DICOM format (angiography mode) of healthy patients without pathology and patients with an anomaly such as aortic aneurysm were used.

Based on the geometry of the vessels of the reconstructed models, basic configurations were constructed that simulate the bifurcation of the abdominal aorta in a healthy state—without aneurysm and with an aneurysm. The diameter of the aorta (parent vessel) was assumed to be 2 cm, which agrees with known physiological data [49]. Let us call the vessels emerging from the bifurcation 'the child vessels'.

The aneurysm is modelled by a sphere located either at some distance from the bifurcation or directly at its node. The aneurysm radius varies in the range from 2.5 to 5 cm, which is also consistent with clinical studies of the detection limits and the maximum size of observation of this pathology [58]. Such a configuration, as mentioned above, makes it possible to exclude the features of the geometry of specific patients in the study of general hydrodynamic effects.

The first of those considered was the configuration in which the aneurysm is located at a distance of 5 cm above the bifurcation.

Several options for the ratio of the radii of the child vessels in the bifurcation were considered: two equal vessels; the radius of one of the vessels is 50% larger

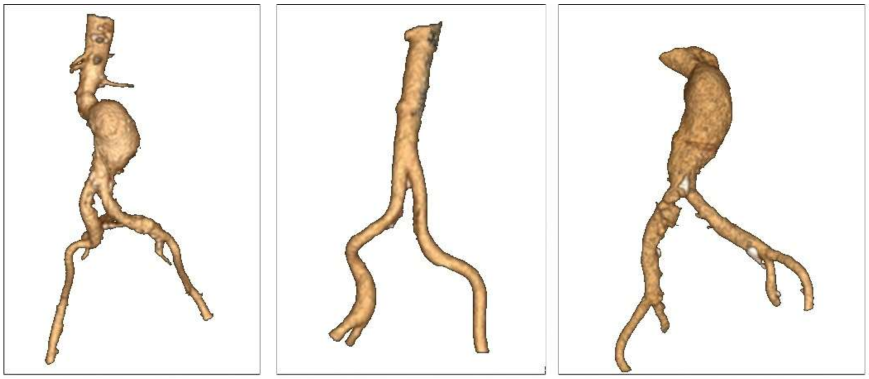

Figure 2. A series of real geometries of the aorta with and without aneurysm based on data of patients of Meshalkin National Medical Research Center of Ministry of Healthcare of The Russian Federation. The reconstruction was performed using the commercial software package Radiant DICOM Viewer (Poland). A total of 30 configurations restored.

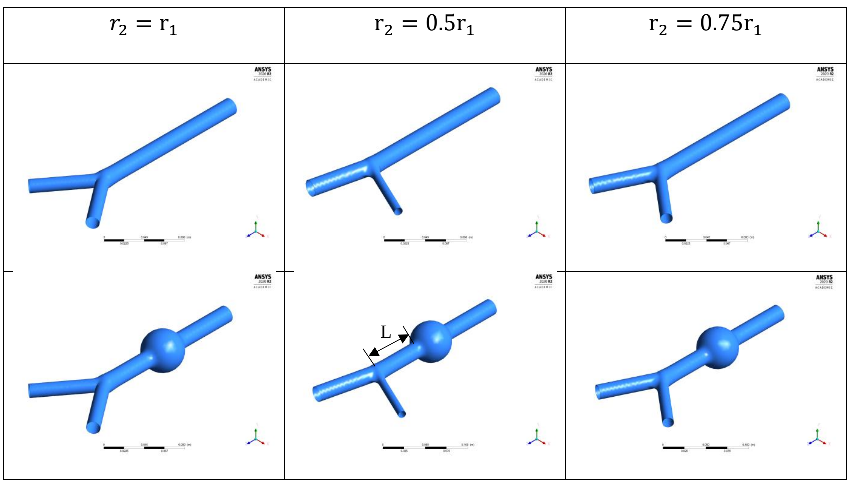

Figure 3. Idealized model configurations for the cases of a healthy aorta (top) and an aneurysm on the aortic trunk (bottom).

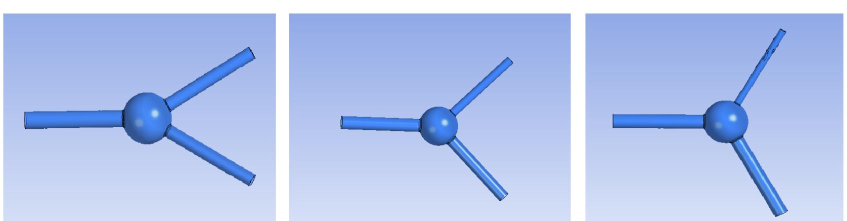

Figure 4. Idealized model configurations for the case of bifurcation aneurysm of the abdominal aorta: $r_2 = r_1$ on the left, $r_2 = 0.75r_1$ in the center, $r_2 = 0.5r_1$ on the right. Bifurcation opening angle 60, 90, and 120 degrees (from left to right).

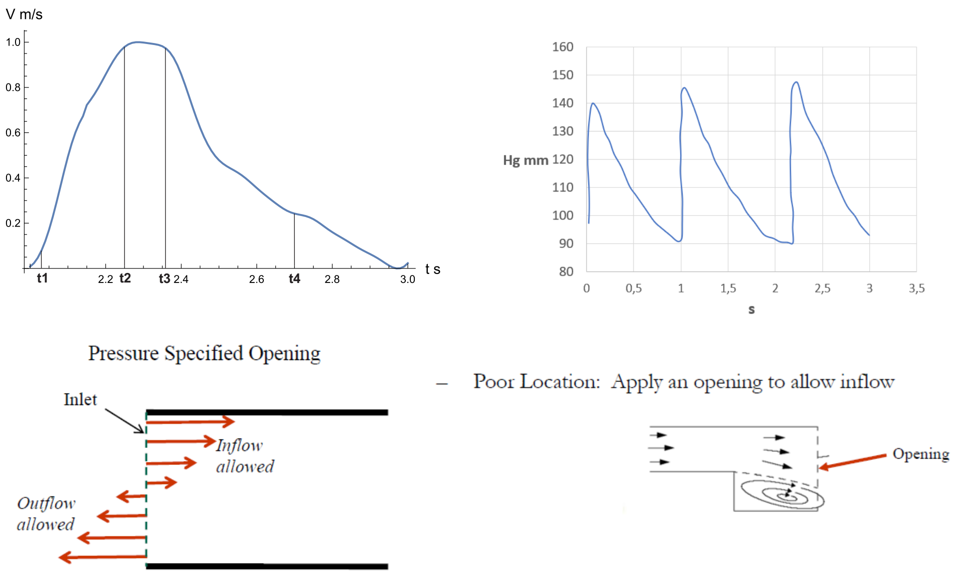

Figure 5. Top row: scaled on the interval $[0,1]$ velocity profile of a real patient (left), pressure profile of a real patient (right). Bottom row: scheme of the boundary condition of the Inlet type (left), scheme of the boundary condition of the Opening type [1] (right).

Table 1. Estimated deviation angles based on Murray's law and equation (1.1).

	$r_2 = r_1$	$r_2 = 0.75r_1$	$r_2 = 0.5r_1$
r_0	1	1	1
r_1	0.8	0.96	0.89
r_2	0.8	0.48	0.67
ϑ_1	37	13	25.5
ϑ_2	37	64.6	50

than the other (significant difference in diameter); the difference in the diameters of the child vessels is 25% (not a significant difference in diameter). To calculate the angle between the child vessels, Murray's law was used, based on a simplified condition for minimizing the total work of the flow when passing through a bifurcation [41, 42]. According to this law, the radii of the parent vessel and the child branches of the bifurcation follow a power law: $r_1^\gamma = r_2^\gamma + r_3^\gamma$, where γ is a branching index, also called bifurcation parameter. Usually $\gamma \approx 3$ is accepted (see [53, 61, 63]). Based on considerations of minimizing the energy loss of the flow at the bifurcation, a formula is derived for the angle ϑ_i between the child and parent vessels [52]:

$$\cos\vartheta_i = \frac{{r_0}^4 + {r_i}^4 - ({r_0}^3 - {r_i}^3)^{4/3}}{2{r_0}^2{r_i}^2}, \quad i = 1, 2. \tag{1.1}$$

By default, we further calculate $r_1 \geqslant r_2$. The calculated values of the cross sections of the vessels according to the assumptions made and formula (1.1) are given in Table 3.

The second model configuration of those considered was the configuration with an aneurysm located directly on the aortic bifurcation (see Fig. 4).

Thus, we studied haemodynamics for two types of geometric configurations: with localization of the aneurysm on the aorta trunk (three configurations without aneurysm and three configurations with aneurysms) and on bifurcation (nine configurations without aneurysm and nine configurations with aneurysms). In each of these types, individual configurations differ in the ratio of the radii of the aorta and iliac arteries and the angles between them.

1.2. Mathematical model and boundary conditions

In a healthy and calm state, the blood flow velocity in the human abdominal aorta during the cardiac cycle varies from 0.2 to 1.8 m/s. Therefore, in the numerical simulation of the flow through the aortic bifurcation model in the steady case, a uniform blood velocity profile of 0.5 m/s was specified at the inlet to the aortic model. This condition for 1 s provides a volume of uniform blood flow comparable to the regime of pulsating blood pumping. At the outlet, both in steady and unsteady cases, a zero pressure value was set (the Opening condition). In the unsteady case, the input was a patient-specific velocity profile in the aorta, measured at the diagnostic stage using an ultrasound measurement unit (*B*-mode). The initial velocity and pressure profiles, as well as the marked time points for which the solution was analyzed, are shown in Fig. 5. The pathway for using patient-specific profiles in unsteady calculation was as follows: a patient-specific velocity profile was set at the inlet and, based on the results of the calculation, a pressure graph was plotted in the selected section. This graph was compared with the data obtained during intraoperative measurement, and the scaling factor for the velocity graph was calculated in this way to minimize the difference between clinical pressure and calculated pressure using the least squares method (LSM). Blood pressure in the aorta was measured as follows: using the Seldiner method under X-ray control, a puncture of the common femoral artery was performed, a 6 Fr Avanti introducer (Cordis, Ireland) was inserted retrogradely; A 6 Fr Ranway jr4 guiding catheter (Boston scientific, USA) was inserted into the area of the ascending aorta using a Radiofocus Guide Ware 0.35 (Terumo, Japan). The measurement was carried out on an Intellie Veu device (Phillips, Germany).

The Navier–Stokes equations for the flow of a viscous incompressible fluid have the following form [59]:

$$\begin{gathered}\sum_{j=1}^{N}\frac{\partial u_j}{\partial x_j}=0\\ \frac{\partial u_i}{\partial t}+\sum_{j=1}^{N}\frac{\partial u_i u_j}{\partial x_j}+\frac{\partial \widehat{p}}{\partial x_i}=\sum_{j=1}^{N}\frac{\partial}{\partial x_j}\mu\left(\frac{\partial u_i}{\partial x_j}+\frac{\partial u_j}{\partial x_i}\right).\end{gathered} \tag{1.2}$$

System (1.2) can be rewritten as

$$\mathbf{R}^t\frac{\partial \mathbf{U}}{\partial t}+\frac{\partial \mathbf{F_1}}{\partial x_1}+\frac{\partial \mathbf{F_2}}{\partial x_2}+\frac{\partial \mathbf{F_3}}{\partial x_3}=0 \tag{1.3}$$

where $\mathbf{R}^t = \operatorname{diag}\big(0,1,1,1\big)$,

$$\mathbf{U}=\begin{pmatrix}p\\u_1\\u_2\\u_3\end{pmatrix},\quad \mathbf{F}_1=\begin{pmatrix}u_1\\{u_1}^2+\widehat{p}-\tau_{11}\\u_1u_2-\tau_{12}\\u_1u_3-\tau_{13}\end{pmatrix},\quad \mathbf{F}_2=\begin{pmatrix}u_2\\u_1u_2-\tau_{12}\\{u_2}^2+\widehat{p}-\tau_{22}\\u_1u_3-\tau_{23}\end{pmatrix}$$
$$\mathbf{F}_3=\begin{pmatrix}u_3\\u_1u_3-\tau_{13}\\u_2u_3-\tau_{23}\\{u_3}^2+\widehat{p}-\tau_{33}\end{pmatrix},\quad \tau_{ij}=\mu\Big(\frac{\partial u_i}{\partial x_j}+\frac{\partial u_j}{\partial x_i}\Big) \tag{1.4}$$

and $\widehat{p}=p/\rho$, $\rho=\text{const}=997$ kg/m^3 is the liquid density, p is pressure, F denotes the external forces acting on the system, $\mathbf{u}=(u_1,u_2,u_3)$ are the velocity vector components, $\mu=0.004$ Pa is the dynamic viscosity of blood [2]. The aorta is the largest vessel of the body and, without loss of generality, the rheology of the blood flowing through it can be considered Newtonian [2].

In the case of an unsteady flow of an incompressible fluid, derivatives with respect to fictitious time t' are added to system (1.3):

$$\frac{\partial\mathbf{U}}{\partial t'}+\mathbf{R}^t\frac{\partial\mathbf{U}}{\partial t}+\frac{\partial\mathbf{F_1}}{\partial x_1}+\frac{\partial\mathbf{F_2}}{\partial x_2}+\frac{\partial\mathbf{F_3}}{\partial x_3}=0 \tag{1.5}$$

where $\mathbf{R}^t = \operatorname{diag}\big(0,1,1,1\big)$.

The standard [30, 31, 57] scheme implemented in the ANSYS CFX 2020R2 [1] package was used for the solution, the number of nodes varied in the range from 22000 to 44000 with a mesh element size of 1 mm and an unstructured tetrahedral mesh , which is the gold standard for calculating the hydrodynamics of flow regions with circulation [1]. The variation of the grid cell sizes showed good convergence of the method in all cases, except for the case of an aneurysm with a radius of 5 cm, when, as we believe, there are geometric features of the grid generation that affect the solution. To correctly implement the no-slip conditions in the numerical formulation, we used a prismatic layer of cells along the walls of the vessel, 5 cells thick with a cell thickness step equal to 2 when approaching the wall. Such a formulation is recommended for describing the flow of a viscous incompressible fluid [1]. We carried out several calculations with a variation of these parameters (the number of layers of the prismatic layer and the ratio of their thickness), which showed the possibility of changing the main haemodynamic quantities (velocities, pressure, shear stresses) in the flow region up to $\approx 20\%$. The formulation of the problem with rigid walls has the right to be considered in view of the physiological aspects of the abdominal aneurysm. The fact is that the structure of the aortic aneurysm wall and its bifurcation contains a large amount of fibrous tissue making the structure much more rigid in vivo, which was confirmed in situ [35], compared to a healthy vessel. This corresponds to the general concept of the need to take into account the fluid-structure interaction (FSI) effects depending on the problem statement [36].

In contrast to the calculation with rigid walls, in the FSI calculation it is necessary to specify the elasticity parameters of this wall (see Table 2). These values were obtained in experiments with aorta and aneurysm samples from real patients [35].

The interaction between the vessel wall and the liquid volume for the entire configuration in the FSI approach is described by the equations

$$\mathbf{v} = \dot{\mathbf{u}}, \qquad \sigma \cdot \mathbf{n}_w + \tau \cdot \mathbf{n}_f = 0 \tag{1.6}$$

where $\mathbf{v}$ is the blood flow velocity, $\dot{\mathbf{u}}$ is the wall motion velocity, σ is the wall stress tensor, τ is the tensor of shear stresses on the wall, $\mathbf{n}_w$ and $\mathbf{n}_f$ are the normals of the wall and fluid, respectively. These equations determine the kinematic and dynamic conditions at the wall–fluid interface, respectively.

The mechanics of the wall as a result of the action of the blood flow on it is modelled using the finite element method.

An adaptive prismatic mesh is used to model the vessel wall. The number of nodes varies from 6300 to 7500 depending on the presence and size of the aneurysm.

At the entrance of the aorta in FSI steady calculation, a blood flow is supplied at a speed of 0.5 m/s. At the exits from the iliac arteries, the Opening condition is set for the correct modelling of possible eddies near the exits. The principle of operation of conditions at the input (Inlet) and outputs (Outlet) is shown in Fig.5.

2. Results

2.1. Steady calculation. Viscous dissipation

Performing a steady calculation is useful for investigating the underlying patterns of the flow. It was carried out with the following boundary conditions: a fixed velocity value was set at the inlet, and zero pressure was set at the outlet of the child vessels. The speed varied from 0.3 m/s to 2.0 m/s, which corresponds to physiological parameters. Despite the fact that the process of blood flow in the abdominal aorta is unsteady, the processes that occur in the wall of this vessel, as well as in its cavity, have a scale of several months - years, and therefore, on the scale of the cardiac cycle, one should not expect those patterns that are not showed themselves in a steady calculation. In addition, in the paper [16] it is shown that to assess the integral flow characteristics in the haemodynamics of large vessels, there is no need to consider an unsteady flow.

In papers [30, 43] the importance of such quantity as viscous dissipation has already been shown. For rigid structures, this value is the only marker for assessing energy losses. In this regard, the study of this quantity seems to be extremely important for the problem under consideration.

The dissipative function (scattering function, viscous energy dissipation function) is introduced to take into account the transition of the energy of ordered motion into the energy of disordered motion [40]. The power that develops in this case per unit of time is calculated by the formula:

$$D = 4\mu \int_{\Omega} |\vec{\omega}|^2 \, \mathrm{d}V \tag{2.1}$$

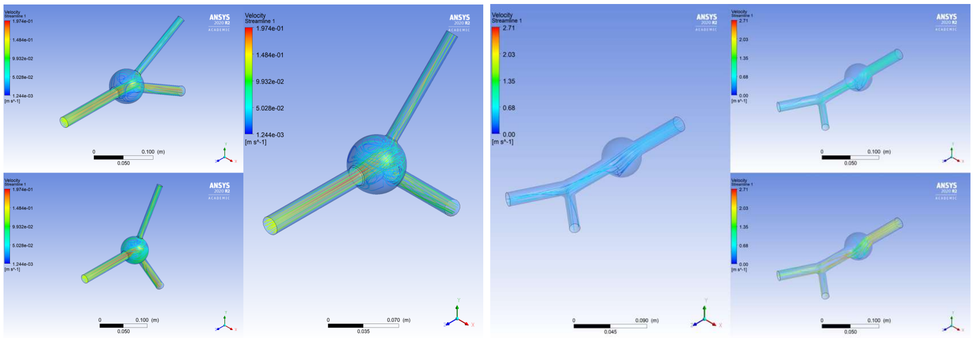

Figure 6. Streamlines in idealized model configurations: a case of an aneurysm on the bifurcation (on the left), an aneurysm on the aortic trunk (on the right).

where $\vec{\omega}$ is the velocity vortex vector, μ is the fluid viscosity, Ω is the flow region, V is the volume of region Ω. This value significantly depends on the volume of the integration domain, while the size of the vortex in the aneurysmal sac is directly related to its volume (see Fig. 6). Therefore, along with the absolute values of the vortex $|\vec{\omega}|$, it is natural to consider its specific:

$$D_{\text{unit}} = \frac{D}{V} \tag{2.2}$$

value (in relation to the calculated volume).

2.2. Unsteady calculation. Pressure surge

During the cardiac cycle, aortic pressure changes significantly (see Fig. 5). Therefore, it seems natural to evaluate the change in pressure in the system during the occurrence and growth of an aneurysm in an unsteady calculation. To study the influence of the aneurysm size on the pressure value in the vessel, we introduce the value $P_{\text{var rel}}$, which is defined by the formula:

$$P_{\text{var rel}} = \frac{P_a - P_n}{P_n} \tag{2.3}$$

where P_a is the pressure in configuration with an aneurysm, P_n is the pressure in configuration without an aneurysm.

This value was calculated for 9 configurations and 16 intermediate bifurcation aneurysm radii. At the entrance to the aorta, a blood flow was supplied with velocity values $v(t_i)$ corresponding to the time points t_1, t_2, t_3, and t_4 in Fig. 5.

In the case of equality of the radii of the child vessels ($r_1 = r_2$), it was numerically obtained that the increase in the radius of the aneurysm is statistically associated with an increase in pressure in the vessels ($p < 0.05$) and can be described using a linear regression model. This effect is shown in Fig. 9. The values of slope, shift, and coefficient of determination are given in Table 4. In other cases, it was not possible to identify a statistically justified linear increase or decrease in pressure

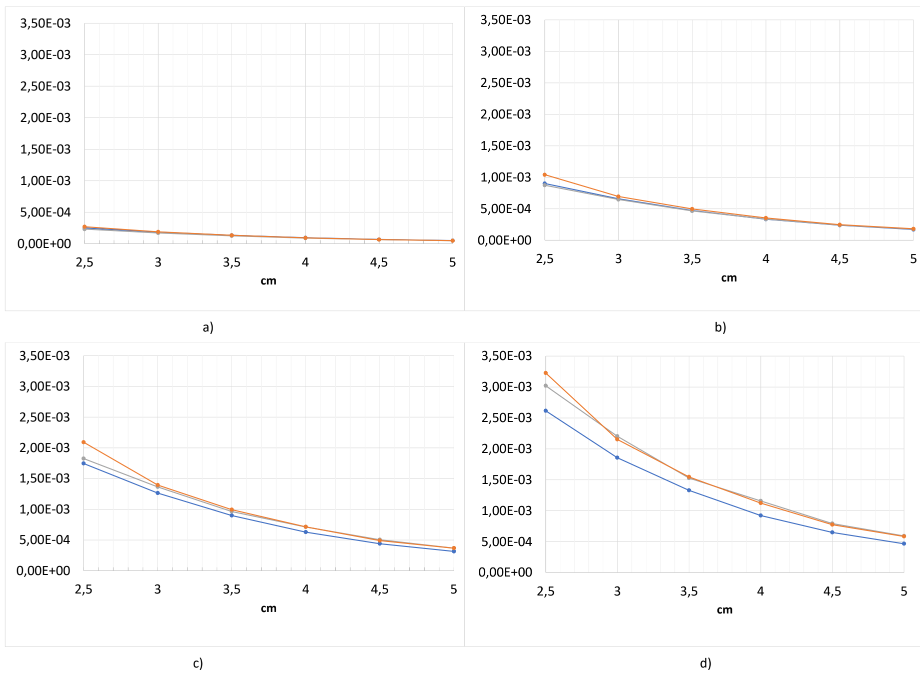

Figure 7. Dependence of the specific dissipation power D_{unit} on the size of the aneurysm in the case of localization of the aneurysm on the aortic trunk at different values of velocity in the aorta: (a) 0.5 m/s; (b) 1.0 m/s; (c) 1.5 m/s; (d) 2.0 m/s.

with increasing aneurysm radius, since the linear regression model did not provide a satisfactory description of the data ($R^2 < 0.3$).

As a result of comparing the values of $P_{\text{var rel}}$ calculated in the models of rigid and elastic vessels, it was found that when passing from the calculation with rigid walls to the FSI calculation, with a difference in absolute and relative values, the trend persists at all considered time points and for all angles of the solution of the iliac arteries. The results obtained are shown in Fig. 11. More detailed results are shown in Fig. 19.

2.3. PV diagrams

Pressure–velocity diagrams (PV diagrams, pressure–velocity loops) are a powerful tool for qualitative analysis in haemodynamics [25, 26, 34]. They make it possible to evaluate the integral characteristics of the entire haemodynamic circuit. In this case, it was of interest to evaluate the integral characteristics of the haemodynamic system ‘blood flow–rigid wall’ with and without an aneurysm in different parts of this circuit: distal (downstream) and proximal (upstream) of the aneurysm.

To calculate the integral characteristic of such a circuit, the area occupied by the PV diagram was calculated. The numerical implementation of this process contained the quadrature formula of trapezoids. Then the ratio of the area of the limited

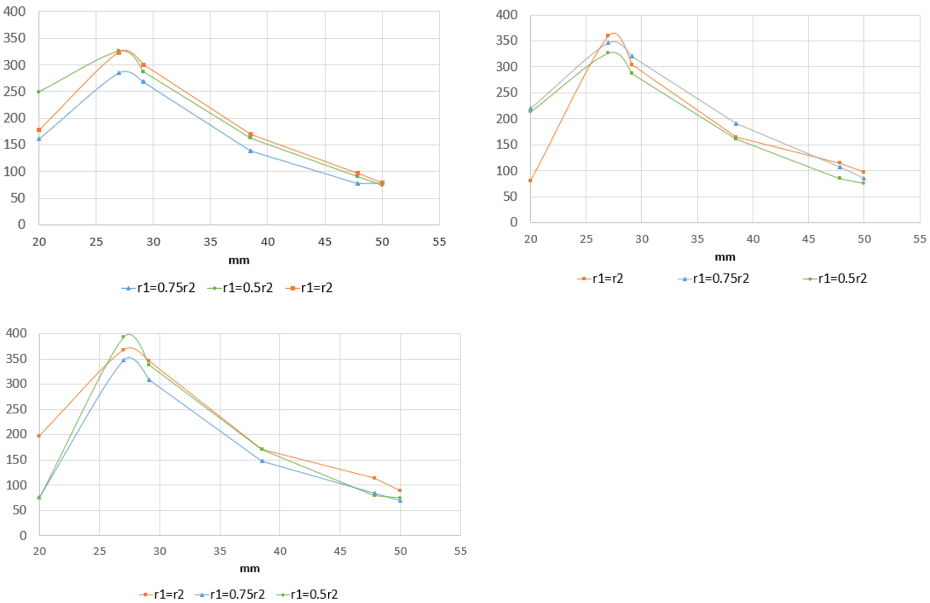

Figure 8. Dependence of the specific dissipation power D_{unit} on the size of the aneurysm in the case of aneurysm localization on the aortic bifurcation at a fixed inlet flow velocity. The opening angle of the iliac arteries: 60° (top left), 90° (top right), and 120° (bottom).

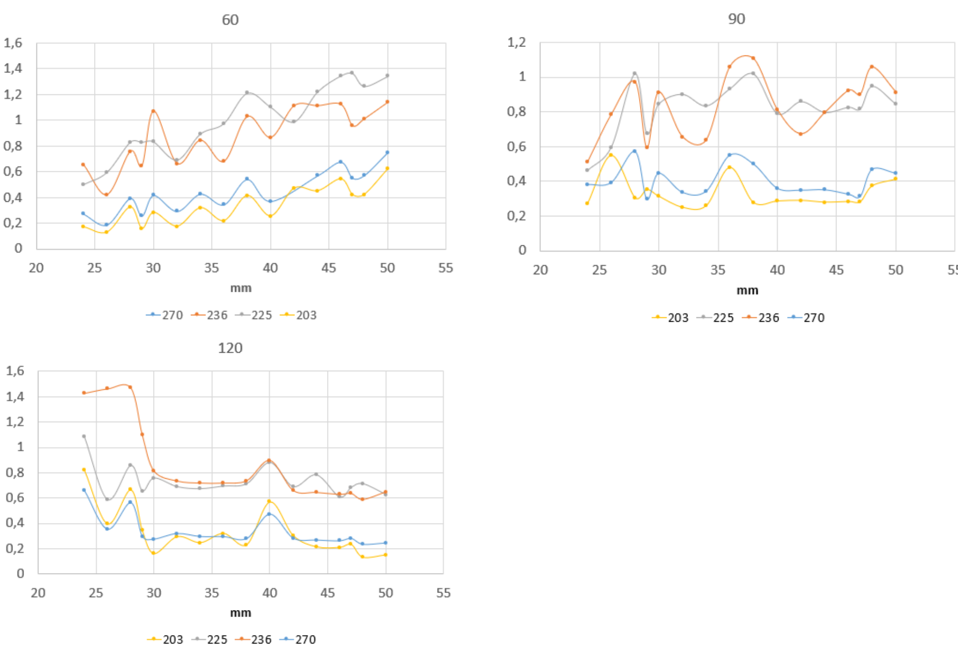

Figure 9. Dependence of $P_{\text{var rel}}$ on aneurysm size for different time points during the cardiac cycle.

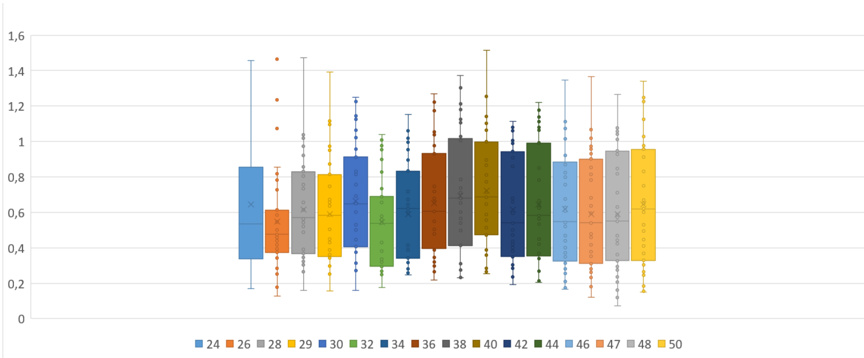

Figure 10. Diagrams of $P_{\text{var rel}}$ values for all considered aneurysm radii.

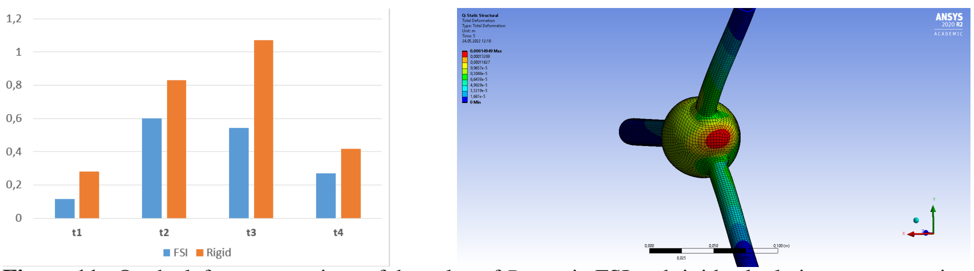

Figure 11. On the left — comparison of the value of $P_{\text{var rel}}$ in FSI and rigid calculations at an opening angle of 60°, on the right — distribution of deformations of the aneurysm wall obtained in the FSI formulation.

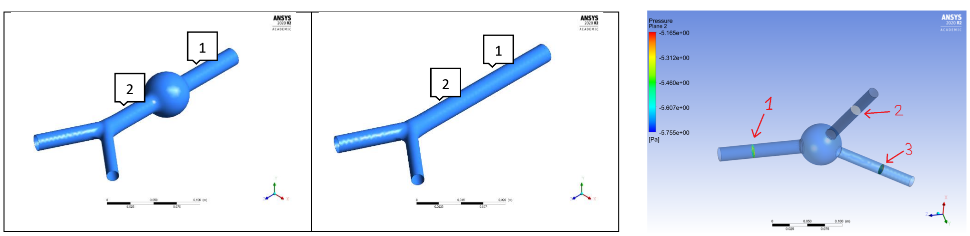

Figure 12. Control sections for model configurations: on the left — an aneurysm on the aortic trunk, on the right — a bifurcation aortic aneurysm.

diagram in the presence of an aneurysm to the same area in the configuration without an aneurysm was found. Let us denote by

$$\mathrm{CW} = S_{\mathrm{PVaneurysm}}/S_{\mathrm{PVhealthy}} \tag{2.4}$$

a value that characterizes the ratio of the area in the presence of an aneurysm to the area without it at the same values of the radii and angles of the configuration. Value (2.4) was calculated in the sections shown in Fig. 12. The data obtained for the bifurcation aneurysm are shown in Fig. 13.

As a result of the calculations, it was found that with an increase in the radius of the aneurysm, the area of the area bounded by PV diagrams proximal to the

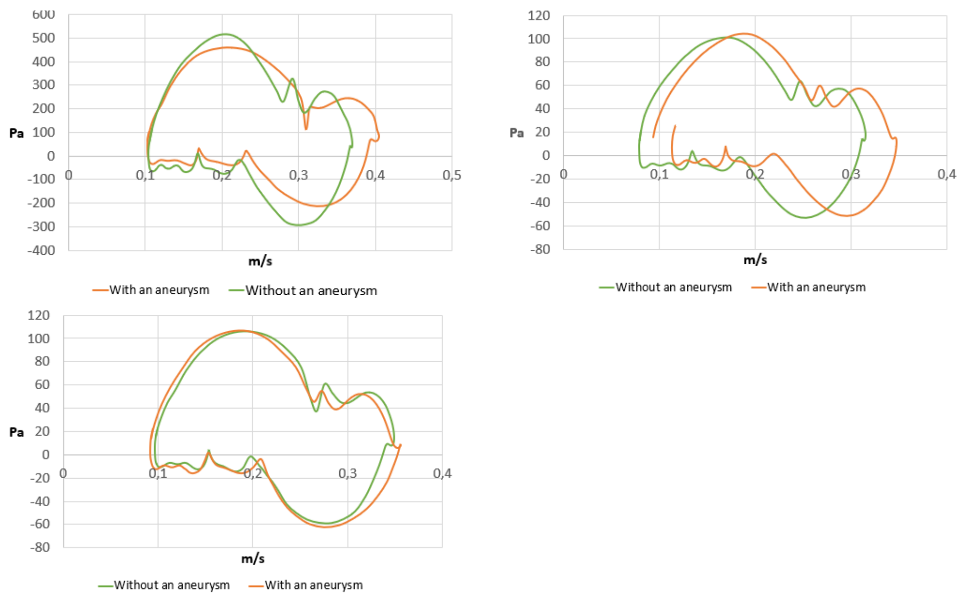

Figure 13. Examples of PV diagrams in the considered configurations.

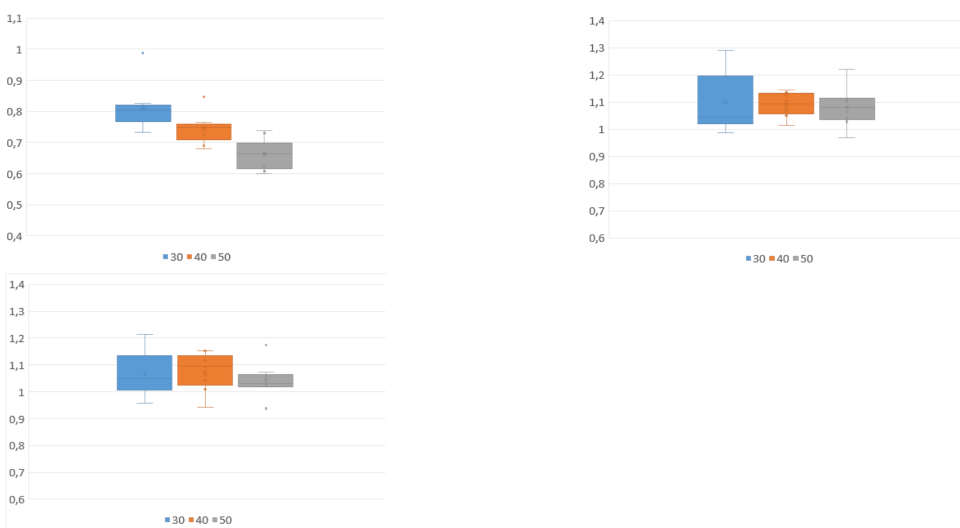

Figure 14. Dependence of the value of CW on the radius of the aneurysm. Plane 1 (top left), plane 2 (top right), and plane 3 (bottom).

aneurysm decreases, and in the iliac arteries (distal to the aneurysm) does not change in all considered configurations. For configurations in which the aneurysm is located on the aortic trunk, PV diagrams and the distribution of CW are shown in Figs. 15 and 16, respectively.

Analysis of the values of CW in the presence of an aneurysm on the aortic trunk

Figure 15. On the left: PV diagrams for a configuration with an aneurysm on the aortic trunk. Configurations with aneurysm are marked in red, without aneurysm in green. On the right: the statistics of the distribution of the CW value for various considered values of the iliac artery radii and the radius of the aneurysm. The first and the second lines are, respectively, the sections above and below the aneurysm along the flow.

Table 2. Wall material parameters.

Thickness	Density	Young's modulus	Poisson's ratio
2 mm	1100 kg/m^3	80000 Pa	0.45

shows that proximal to the aneurysm, with its growth, the area of the region bounded by the diagram decreases, and distally it does not change significantly. In addition, one can notice a qualitative difference between the diagrams for the configuration with a bifurcation aneurysm and an aneurysm on the trunk. In the first case, a phase shift is present in the PV diagram (bumps in the lower part of the graph), which corresponds to the 'plateau' section on the patient-specific velocity profile graph (the flattest section between points T_3 and T_4 (see Fig.5).

A study of the evolution of the slope of the PV diagram for the configuration with an aneurysm on the trunk shows that with its growth distal to the aneurysm, no changes in the slope with the growth of the aneurysm are observed. Proximal to the aneurysm, the ratio of the tangents of the inclination angles tends to 0 with the growth of the aneurysm, which means that the influence of the aneurysm on the 'working' characteristics of the haemodynamic complex vessel–bifurcation–aneurysm is vanished.

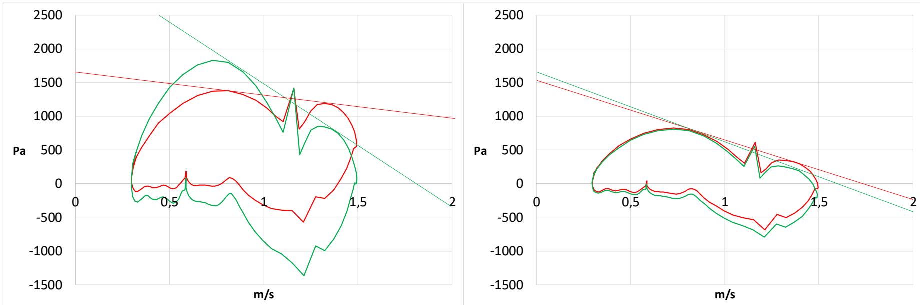

Figure 16. Top: PV diagrams with tangents to them for a configuration with an aneurysm on the aortic trunk: a section before the aneurysm (on the left), a section after the aneurysm (on the right). (Cases with aneurysms are in red, those without aneurysms are in green). Bottom: change in the tangent of the tangent to the PV diagram when the flow passes through the aneurysm.

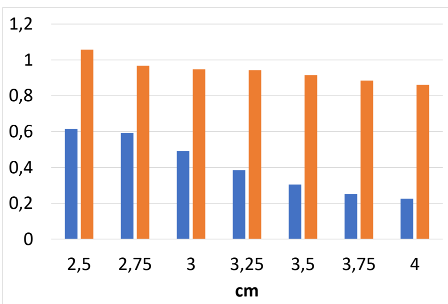

Figure 17. Change in the tangent of the slope of the tangent to the PV diagram: the values for the section before the aneurysm are shown in blue, the values for the section after the aneurysm are shown in orange.

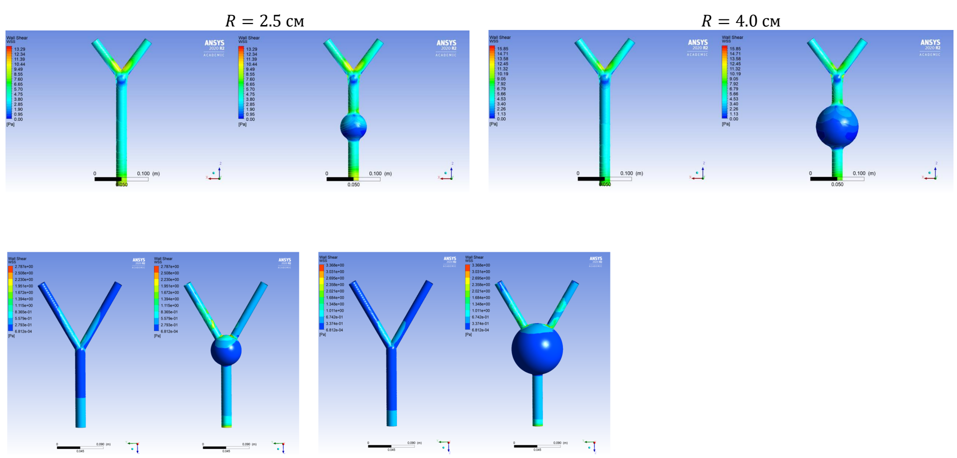

Figure 18. Shear stresses on the vessel wall in model configurations. Top: a case of aneurysm on the aortic trunk, bottom: an aneurysm on the aortic bifurcation.

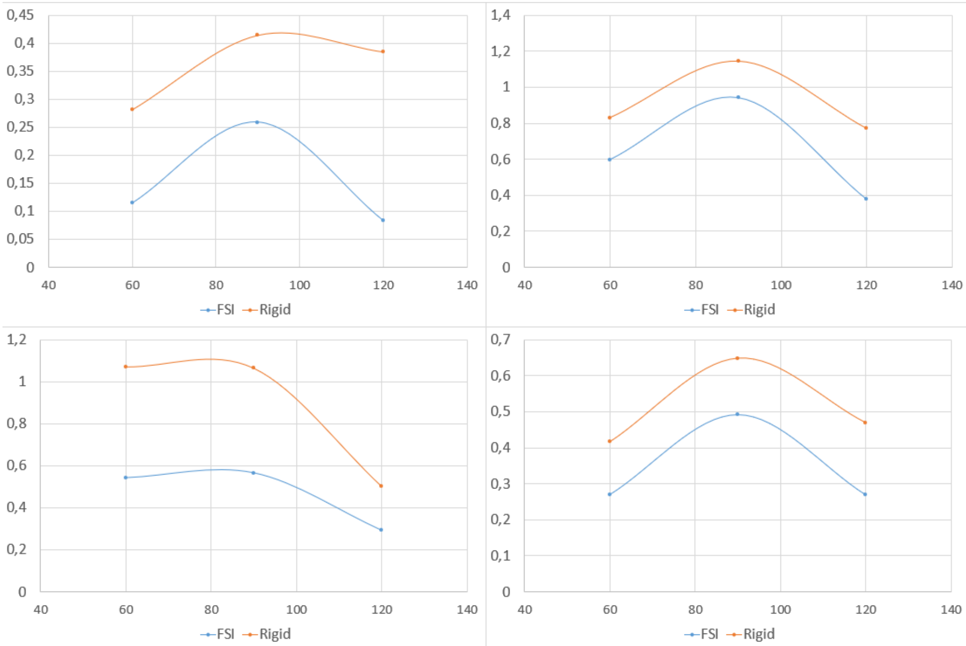

Figure 19. Graphs of the $P_{\text{var rel}}$ value in rigid and FSI calculations. Top row: velocity corresponds to t_1 (left), velocity corresponds to t_2 (right). Bottom row: velocity corresponds to t_3 (left), velocity corresponds to t_4 (right).

Table 3. PV diagrams combined by configurations with aneurysm on the aortic trunk (red) and without (green), the aneurysm radius equals 4 cm.

	Sections	
$r_2 = r_1$	$r_2 = 0,75r_1$	$r_2 = 0,5r_1$
	Before the aneurysm	
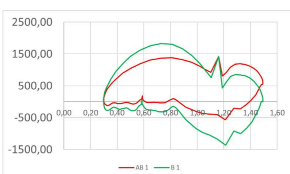	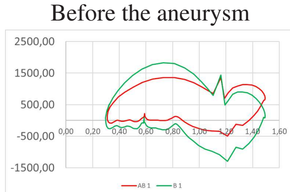	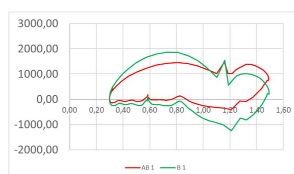
	After the aneurysm	
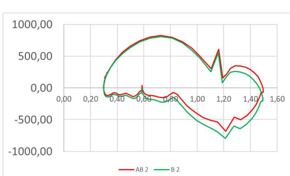	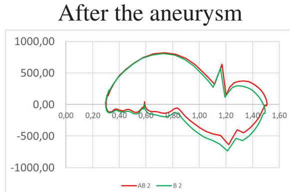	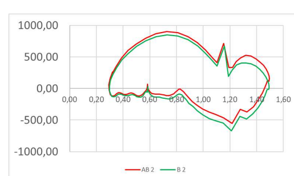

3. Discussion

Vessel bifurcation is a common element of hydrodynamic systems of both natural and engineering origin. This is the branching of blood vessels, and the branching of

Table 4. Configuration linear regression coefficients $r_1 = r_2$.

	Angles	Slope	Shear	Coefficient of determination
Step 203	60	−0.015	0.217	0.726
	90	0.008	0.642	0.153
	120	−0.01	0.686	0.399
Step 225	60	0.0308	−0.144	0.882
	90	−0.004	1.288	0.052
	120	−0.004	1.288	0.280
Step 236	60	0.02	0.131	0.593
	90	−0.0007	1.11	0.002
	120	−0.002	0.6	0.015
Step 270	60	0.017	−0.169	0.775
	90	−0.009	0.84	0.166
	120	−0.005	4.224	0.009

river beds in the delta, and the branching crown of a tree. A characteristic feature of these systems is the bifurcation: the branching of the parent channel into two child branches. The energy of a wave that has passed a branch node in a linear approximation is inversely proportional to the number of child branches, so the general principle of the minimum of lost, reflected energy leads precisely to a bifurcation. It is of interest that bifurcation is characteristic even for branching of vessels in their abnormal development such as arteriovenous malformation [44]. At the same time, one of the anomalies of the blood vessels of the ascending aortic arch is the branching of the vessels into more than two child branches, the so-called ‘bull vessel’ [22]. When designing pipelines for various purposes, engineering formulas are used for calculating the interfaces of pipes of various diameters at various angles [21]. In modern theoretical hydrodynamics, the problem of flow in a bifurcation, channel branching has not been fully resolved. The variable parameters of such a system are the sections of the parent and child pipes, the opening angle of the child pipes, the flow parameters — the speed and pressure at the inlet, the Reynolds number for the flow of a viscous fluid. There is a large number of works devoted to the numerical simulation of flow in bifurcation and blood vessel models [33, 50, 55]. Calculations and experiments demonstrate the presence of an extremely complex flow pattern with eddies and secondary flows, the possibility of blocking the child channel. There is a very limited number of exact results such as effects, general patterns of flow in such systems, for example, Dean vortices [13]. Generally, there are also no theorems that consider the correctness of the formulation of the corresponding initial-boundary value problem, even in the formulation with rigid walls, not to mention the most realistic for applications FSI formulation. For the percolation problem, such a formulation was studied in the papers [7, 46]. This is a source of questions and discussions when setting the boundary conditions at the inlet to the parent tube and the outlets of the child tubes in computer simulation and comparison with experimental, clinical data. The quantities that could be measured by medical devices are velocity (volume flow) and pressure. At the same time, it is clear that these are not the values which control the flow through the bifurcation directly.

There is only one integral conservation law — the principle of mass conservation, i.e., fluid flow in the parent and child pipes. Its implementation for a steady flow is beyond doubt, but even for a pulsating flow, the question of the ratio of the periods of the flow at the inlet and outlet (phase shift) arises. Even more questions and discussions are caused by the formulation of the principle of energy conservation, which certainly depends on the properties of the modelled system and the effects of energy dissipation. It seems that the flow energy losses due to viscous dissipation caused by the vortex formation mechanism play a significant role here [23, 30, 31]. An important role is played by the assessment of the contribution of various components to the total energy of the system. For a model of a cerebral vessel with a fusiform aneurysm with a bleb developing on it, such an approach that considers FSI formulation was presented in [37, 38].

At the same time, there is a need for relatively simple models and laws that, at least approximately, but describe the patterns of flow through the bifurcation. Murray's laws [41, 42], which relate the parameters of a tee: cross-sections of channels, the opening angle of child branches, are widespread and generally accepted. These relations are obtained from very simplified considerations of minimizing the energy loss of the flow during the passage of the branch node (assuming an irrotational Poiseuille flow). Although these assumptions are not satisfied in the bifurcation problem, Murray's laws are used in modern works as some simple relations, which are a kind of zero approximation for more complex models [32]. As mentioned above, the question of the form of the energy relation in the bifurcation problem is a subject of discussion in the literature.

The main purpose of modelling is to find dimensionless parameters that control the behavior of such a complex system, switching it from one mode to another. Examples of building such maps for specific configurations are available in [9]. It seems that a dynamical system which describes such a configuration in a broad sense has mathematical bifurcation points and unstable modes for certain values of [54] parameters. As mentioned above, the quantities actually measured in the clinic are pressure and velocity. There are various techniques for obtaining such data. The relationship of these quantities in blood vessels of various types is an important characteristic of the local circulation. Pressure–velocity diagrams [25, 26, 34], also called PV loops, are used to characterize different modes of the heart [20] circulation. The PV diagram apparatus has been developed and effectively used in neurosurgical blood flow monitoring [26, 39] to detect and visualize abnormalities such as cerebral aneurysms and arteriovenous malformations. It allowed to evaluate the effectiveness of neurosurgical operations. The application of such diagrams to the analysis of various haemodynamic indices are shown in [8, 56]. Despite the fact that the authors of these works are skeptical about the analysis of the area of such diagrams, we believe that it still correlates with the work of the haemodynamic circuit, since we observe a monotonic behavior of this value with aneurysm growth, and we also observe a monotonic change in this value in the case of cerebral haemodynamics in the treatment of cerebral aneurysm, in the analysis of intravascular measurements [25]. From the point of view of continuum mechanics, these diagrams demonstrate a kind of equations of state for a complex system ‘blood flow, vessel wall, and its environment’. The results of numerical analysis of the above monitoring data were described in [38]. For cerebral vessels, these diagrams informatively describe the different impact of the anomaly on the flow both upstream and downstream of it. It seems that the apparatus of PV diagrams is a promising tool for describing the control of a complex system with a bifurcation and the relation of clinical data with a computational experiment.

Note that in our work there are a number of limitations, the removal of which is a substantial non-trivial work. So, for example, we used a spherical shape of the aneurysm, while from the clinical data it follows that the abdominal aortic aneurysm is more like an ellipsoid in shape. In addition to the complexity of constructing such a model geometry, the question arises of interpreting the results obtained. The fact is that the clinically accepted characteristic of an aortic aneurysm is its diameter in the widest part [29]. For a sphere, we can uniquely relate this value to its radius, while in the case of an ellipsoid, the situation becomes much more complicated, since two more parameters appear that control the geometry of the model abdominal aneurysm. At the same time, taking into account the results obtained in [48], it becomes obvious that the use of an ellipsoid or ovoid shape of a model aneurysm provide dramatically different results. Another limitation of our work is that we do not consider the interaction between the thrombus and the vessel wall (see Fig. 1). The cross section of the flow area in our case is the vessel lumen. At the same time, a thrombus in an abdominal aneurysm can be at different stages of maturation and growth, and this does not directly correlate with its size. In the course of rheometric tests on the Anton Paar unit (Austria), we found that the material of such blood clots has viscoelastic properties ten times different for blood clots with different stages of maturation. The study of the process of thrombus formation is a separate problem that is difficult both from the experimental and mathematical points of view [6, 18, 19]. For one of the stages of thrombus development, the characteristics (elastic modulus and loss modulus) are close to those of the aortic aneurysm wall. Thus, we believe that the thrombus and the wall represent a single complex, which is considered ‘simply’ as a wall in our numerical calculations. Meanwhile, the consideration of the vessel wall as a multilayer coating [11, 12] bear a ‘zoo’ of problems in modelling aortic aneurysms of both the abdominal and thoracic segments, both in the experimental aspect and in the sense of mathematical modelling. The mechanical properties of such coatings can be investigated, for example, by the methods used in [27, 28]. The novelty of our approaches compared to the modelling approaches described, for example, in [51] is in the study of the influence of bifurcation, as well as in the assessment of pressure growth proximal to the aneurysm in the presence of aortic bifurcation. It not only significantly complicates the solution, but also raises many questions about the formulation of correct boundary conditions that would make the model formulation close to the clinical one. Separately, we would like to note the use in this work of the laminar flow model in the formulation of the problem. The fact is that for the blood flow in the abdominal segment of the aorta, both with an aneurysm and without it, it is difficult to unequivocally state that there are only areas of laminar flow, or formed areas with a turbulent flow. There are studies in this direction [62], and in the future this aspect will be given special attention.

4. Conclusion

Three model configurations of the abdominal aorta were studied: a healthy aorta, an aorta with an aneurysm on the trunk, and an aorta with a bifurcation aneurysm. For each of these configurations, variations in the opening angle of the iliac arteries and their diameters, as well as variation in the size of the aneurysm, were considered. The basic haemodynamic parameters were calculated both in steady (in rigid and FSI) and in unsteady formulations. A function of viscous dissipation and PV (pressure–velocity)-diagrams were calculated and analyzed. In one of the reference configurations, a linear increase in pressure proximal to the aneurysm relative to the growth of the aneurysm was detected and statistically confirmed ($p < 0.05$). Such dependence may characterize the effect of abdominal aneurysm upstream on the cardiac activity of the myocardium known in the literature, which is confirmed by statistics [17]. This influence is still not unequivocally recognized by the medical community due to the small number of studies in this area. The evidence of such an effect will make it possible to identify patients in the early stages of the development of aortic pathology who have the greatest predisposition to the development of anomalies of cardiac function. In addition, it was found that both for an aneurysm on the trunk and for a bifurcation aneurysm, a proximal decrease in the area of the area limited by PV diagrams with aneurysm growth is characteristic, which is a new and interesting result that motivates for further investigations in this area.

References

1. *ANSYS Documentation, ANSYS CFX-Solver Theory Guide.* ANSYS, Inc. http://www.ansys.com/

2. O. K. Baskurt, M. R. Hardeman, M. W. Rampling, and H. Meiselman, Handbook of Hemorheology and Hemodynamics. *Biomedical and Health Research* **69** (2007).

3. K. A. Beklemysheva, A. A. Danilov, I. B. Petrov, V. Yu. Salamatova, and Yu. V. Vassilevski, Virtual blunt injury of human thorax: age-dependent response of vascular system. *Russ. J. Numer. Anal. Math. Modelling* **30** (2015), No. 5, 259–268.

4. C. Berry, P. Burns, et al., MRI using ultrasmall superparamagnetic particles of iron oxide in patients under surveillance for abdominal aortic aneurysms to predict rupture or surgical repair: MRI for abdominal aortic aneurysms to predict rupture or surgerythe MARS study. *Open Heart* **2** (2015).

5. R. L. T. Bevan, I. Sazonov, and P. H. Saksono, Patient-specific blood flow simulation through an aneurysmal thoracic aorta with a folded proximal neck. *Numerical Methods in Biomedical Engineering* **27** (2011), No. 8, 1167–1184.

6. J. Biasetti, F. Hussain, and T. C. Gasser, Blood flow and coherent vortices in the normal and aneurysmatic aortas: a fluid dynamical approach to intra-luminal thrombus formation. *J. R. Soc. Interface* **8** (2011), 1449–1461.

7. S. Canic, Fluid-structure interaction in incompressible, viscous fluids. In: *Springer's CIME Lecture Notes (Analysis Series) 'Progress in Mathematical Fluid Dynamics'* (Eds. M. Ruzicka and L. Berselli), 2020.

8. J. A. Chirinos and P. Segers, Noninvasive evaluation of left ventricular afterload: part 2: arterial pressure-flow and pressure-volume relations in humans. *Hypertension* **56** (2010), 563–570.

9. P. G. Correa, J. R. Mac Intyre, J. M. Gomba, M. A. Cachile, J. P. Huilin, and H. Auradou, Three-dimensional flow structures in Xshaped junctions: Effect of the Reynolds number and crossing angle. *Phys. Fluids* **31** (2019), 1–13.

10. M. M. Chowdhury, L. P. Zieliski, J. J. Sun, S. Lambracos, J. R. Boyle, S. C. Harrison, J. H. F. Rudd, and P. A. Coughlin, Calcification of thoracic and abdominal aneurysms is associated with mortality and morbidity. *Eur. J. Vasc. Endovasc. Surg.* **55** (2018), 101–8.

11. A. E. Darzhain, A. V. Boiko, V. M. Kulik, and A. P. Chupahin, Analysis of stability of the boundary layer on a flat plate under a finite-thickness two-layer compliant coating. *J. Appl. Mech. Tech. Phys.* **60** (2019), No. 4, 620–630.

12. A. E. Darzhain, A. V. Boiko, V. M. Kulik, and A. P. Chupahin, Parametric investigation of hydrodynamic stability of a boundary layer on a flat plate over two-layer compliant coatings. *Thermophysics and Aeromechanics* **27** (2020), 189–200.

13. W. R. Dean, Note of the motion of fluid in a curved pipe. *Phil. May.* **20** (1997), No. 4, 208–223.

14. T. Dobroserdova, F. Liang, G. Panasenko, and Yu. Vassilevski, Multiscale models of blood flow in the compliant aortic bifurcation. *Applied Mathematics Letters* **93** (2019), 98–104.

15. T. C. Gasser, M. Auer, F. Labruto, J. Swedenborg, and J. Roy, Biomechanical rupture risk assessment of abdominal aortic aneurysms: model complexity versus predictability of finite element simulations. *Eur. J. Vasc. Endovas. Surg.* **40** (2010), 176–185.

16. A. J. Geers, I. Larrabide, H. G. Morales, and A. F. Frangi, Approximating hemodynamics of cerebral aneurysms with steady flow simulations. *J. Biomech.* **47** (2014), 178–185.

17. E. Georgakarakos, C. V. Ioannou, Y. Kamarianakis, Y. Papaharilaou, T. Kostas, E. Manousaki, and A. N. Katsamouris, The role of geometric parameters in the prediction of abdominal aortic aneurysm wall stress. *Eur. J. Vasc. Endovasc. Surg.* **39** (2010), No. 1, 42–48.

18. R. Gottlob and R. May, Experimental thrombosis similar to clinical conditions produced on the hind-legs of minor laboratory animals. *Angiology* **5** (1954), No. 5, 307–311.

19. L. A. Harker, A. B. Kelly, and S. R. Hanson, Experimental arterial thrombosis in nonhuman primates. *Circulation* **83** (1991), No. 6, 41–55.

20. A. Hong, J. Joachim, C. Buxin, C. Lev, A. Le Gall, and S. Millasseau, Using velocity-pressure loops in the operating room: a new approach of arterial mechanics for cardiac afterload monitoring under general anesthesia. *American Journal of Physiology-Heart and Circulatory Physiology* **317** (2019), No. 6, H1354–H1362.

21. I. E. Idelchik, *Handbook of Hydraulic Resistances*. Mashinostroenie Publishing House, 1975.

22. Yi. Inan, Yu. Inan, and H. Ay, The effect of demographic features on aortic arch anatomy and its role in the etiology of cerebrovascular disease. *Neuropsychiatric Disease and Treatment* **14** (2018), 29-35.

23. A. K. Khe, A. P. Chupakhin, A. A. Cherevko, Sh. Sh. Eliava, and Yu. V. Pilipenko, Viscous dissipation energy as a risk factor in multiple cerebral aneurysms. *Russ. J. Numer. Anal. Math. Modelling* **30** (2015), No. 5, 277–287.

24. A. K. Khe, A. A. Cherevko, A. P. Chupakhin, A. L. Krivoshapkin, and K. Yu. Orlov, Endovascular blood flow measurement system. *Journal of Physics: Conference Series* 722 (2016).

25. A. K. Khe, A. A. Cherevko, A. P. Chupakhin, and A. L. Krivoshapkin, Hemodynamic monitoring of cerebral vessels. *J. Appl. Math. Tech. Phys.* **58** (2017), 763–770.

26. A. K. Khe, A. A. Cherevko, A. P. Chupakhin, A. L. Krivoshapkin, K. Yu Orlov, and V. A. Panarin, Monitoring of hemodynamics of brain vessels. *J. Appl. Mech. Tech. Phys.* **58** (2019), No. 5, 763–770.

27. V. M. Kulik, A. V. Boiko, B. Seoudi, et al., Measurement method of complex viscoelastic material properties. *Int. J. Solids Struct.* **47** (2010), No. 3, 374–382.

28. V. M. Kulik and A. V. Boiko, Physical principles of methods for measuring viscoelastic properties. *J. Appl. Mech. Tech. Phys.* **59** (2018), No. 5, 874–885.

29. A. Kumar, P. Persaud, A. F. Leite, and N. Aoyama, Aortic aneurysm: clinical findings, diagnostic and treatment. *Aortic Aneurysm – Clinical Findings, Diagnostic, Treatment and Special Situations*, 2021, 1–16.

30. Yu. O. Kuyanova, S. S. Presnyakov, A. V. Dubovoi, A. P. Chupakhin, and D. V. Parshin, Numerical study of the tee hydrodynamics in the model problem of optimizing the low-flow vascular bypass angle. *J. Appl. Mech. Tech. Phys.* **60** (2019), 1038–1045.

31. Iu. O. Kuianova, A. V. Dubovoy, and D. V. Parshin, Towards the numerical assessment in solving the problem of the effectiveness of vascular anastomosis in neurosurgical operations. *J. Physics: Conference Series* 1359 (2019), 1–7.

32. H. H. S. Lakshmanan, J. J. Shatzel, S. R. Olson, O. J. T. McCarty, and J. Maddala, Modeling the effect of blood vessel bifurcation ratio on occlusive thrombus formation. *Comput. Methods Biomech. Biomed. Engrg.* **22** (2019), No. 11, 972–980.

33. I. Lashgari, O. Tammisola, V. Citro, M. P. Juniper, and L. Brandt, The planar X-junction flow: stability analysis and control. *J. Fluid Mechanics* **753** (2014), 1–28.

34. A. Le Gall, . Gayat, J. Joachim, et al., Velocity-pressure loops can estimate intrinsic and pharmacologically induced changes in cardiac afterload during non-cardiac surgery. An observational study. *Journal of Clinical Monitoring and Computing* (2011), 545–555.

35. A. I. Lipovka, A. A. Karpenko, A. P. Chupakhin, and D. V. Parshin, Strength properties of abdominal aortic vessels: experimental results and perspectives. *J. Appl. Mech. Tech. Phys.* **63** (2022), No. 2, 251–258.

36. A. Lozovskiy, M. A. Olshanskii, and Yu. V. Vassilevski, Analysis and assessment of a monolithic FSI finite element method. *Computers & Fluids* **179** (2019), 277–288.

37. M. Yu. Mamatyukov, A. K. Khe, D. V. Parshin, P. I. Plotnikov, and A. P. Chupakhin, On the energy of a hydroelastic system: Blood flow in an artery with a cerebral aneurysm. *J. Appl. Mech. Tech. Phys.* **60** (2019), 977–988.

38. M. Yu. Mamatyukov, A. K. Khe, D. V. Parshin, and A. P. Chupakhin, Energy approach to the solution of the hydroelastic problem of diverticulum growth on fusiform aneurysm. *J. Appl. Mech. Tech. Phys.* **61** (2020), 866–877.

39. G. Metry, M. Spittle, Sh. Rahmati, F. Ronco, C. Ronco, and N. W. Levin, Online monitoring of cerebral hemodynamics during hemodialysis. *Original Investigations: Dialysis Therapies* **40** (2002), No. 5, 996–1004.

40. L. M. Milne-Thompson, *Theoretical Hydrodynamics*. London, MoM and Co LTD; New York, St. Mahnis Press, 1960.

41. C. D. Murray, The physiological principle of minimum work: I. The vascular system and the cost of blood volume. *Proc. of the National Academy of Sciences of the United States of America* **12** (1926), No. 3, 207–214.

42. C. D. Murray, The physiological principle of minimum work: II. Oxygen exchange in capillaries. *Proc. of the National Academy of Sciences of the United States of America* **12** (1926), No. 5, 299–304.

43. F. Mut, R. Lhner, A. Chien, S. Tateshima, F. Viuela, Ch. Putman, and J. R. Cebral, Computational hemodynamics framework for the analysis of cerebral aneurysms. *Numerical Methods in Biomedical Engineering* **27** (2011), No. 6, 822–839.

44. K. Orlov, V. Panarin, A. Krivoshapkin, and D. Kislitsin, Assessment of periprocedural hemodynamic changes in arteriovenous malformation vessels by endovascular dual-sensor guidewire. *Interventional Neuroradiology* **21** (2015), No. 1, 101–107.

45. A. Piechota-Polanczyk, A. Jozkowicz, W. Nowak, W. Eilenberg, C. Neumayer, T. Malinski, I. Huk, and C. Brostjan, The abdominal aortic aneurysm and intraluminal thrombus: current concepts of development and treatment. *Front. Cardiovasc. Med.* (2015), 2–19.

46. P. I. Plotnikov and J. F. Toland, Modelling nonlinear hydroelastic waves. *Philosophical Transactions of the Royal Society A - Mathematical Physical and Engineering Sciences* **369** (2011), 2942–2956.

47. A. Polanczyk, A. Piechota-Polanczyk, L. Stefaczyk, and M. Strzelecki, Spatial configuration of abdominal aortic aneurysm analysis as a useful tool for the estimation of stent-graft migration. *Diagnostics* **10** (2020), No. 10, 737.

48. Yue Qui and Jiarong Wang, Association between blood flow pattern and rupture risk of abdominal aortic aneurysm based on computational fluid dynamics. *Eur. J. Vasc. Endovas. Surg.* **20** (2020).

49. N. Sakalihasan, H. Kuivaniemi, B. Nusgens, R. Durieux, and J.-O. Defraigne, *Aneurysm: Epidemiology Aetiology and Pathophysiology*. Springer, 2018.

50. A. M. Sapardi, W. K. Hussam, A. Pothrat, and G. J. Sheard, Linear stability of confined flow around a 180-degree sharp bend. *J. Fluid Mechanics* **822** (2017), 813–847.

51. I. Sazonov, A. W. Khir, and W. S. Hacham, A novel method for non-invasively detecting the severity and location of aortic aneurysms. *Biomechanics and Modeling in Mechanobiology* **16** (2017), 1225–1242.

52. E. Sciubba, A critical reassessment of the Hess–Murray law. *Entropy* **18** (2016), 283.

53. T. F. Sherman, On connecting large vessels to small. The meaning of Murray's law. *J. General Physiology* **78**, No. 4, 431–53.

54. L. P. Shilnikov, A. L. Shilnikov, D. V. Turaev, and L. O. Chua, Methods of qualitative theory in nonlinear dynamics, Part I, II. *World Scientific Co. Pte. Ltd.* (1998), 392.

55. F. T. Smith, Fluid flow into a curved pipe. *Proceedings of the Royal Society of London. Series A, Mathematical and Physical Sciences* **351** (1976), No. 1664, 71–87.

56. D. P. Stonko, J. Edwards, and H. Abdou, A technical and data analytic approach to pressure-volume loops over numerous cardiac cycles. *JVS-Vascular Science* **3** (2020), 73–84.

57. D. Tikhvinskii, Y. Kuianova, D. Kislitsin, et al., Numerical assessment of the risk of abnormal endothelialization for diverter devices: clinical data driven numerical study. *J. Pers. Med.* **12** (2022), No. 4, 652.

58. G. R. Upchurch Jr. and T. A. Schaub, Abdominal aortic aneurysm. *University of Michigan Health System* Michigan, **73** (2006), No. 7, 1198–1204.

59. Yu. Vassilevski, M. Olshanskii, S. Simakov, and A. Korobov, Personalized computational hemodynamics. Models, methods and application for vascular surgery and antitumor therapy. *Elsevier*, 2020.

60. A. Wanhainen et al., European Society for Vascular Surgery (ESVS) 2019 Clinical Practice Guidelines on the Management of Abdominal Aorto-iliac Artery Aneurysms. *Eur. J. Vasc. Endovasc. Surg.* (2018), 8–93.

61. H. R. Williams, R. S. Trask, P. M. Weaver, and I. P. Bond, Minimum mass vascular networks in multifunctional materials. *J. Royal Society Interface* **5** (2008), No. 18, 55–65.

62. L. Xu, T. Yang, L. Yin, Y. Kong, Yu. Vassilevski, and F. Liang, Numerical simulation of blood flow in aorta with dilation: a comparison between laminar and LES modeling methods. *Computer Modeling in Engineering & Sciences* **124** (2020), No. 2, 1–18.

63. X. Zheng et al., Bio-inspired Murray materials for mass transfer and activity. *Nat. Commun.* **8** (2017), No. 1, 1–9.